Journal of Molecular Graphics and Modelling 28 (2009) 102–112

Contents lists available at ScienceDirect

Journal of Molecular Graphics and Modelling

journal homepage: www.elsevier.com/locate/JMGM

CheckDen, a program to compute quantum molecular properties on spatial grids

Luis F. Pacios *, Alberto Fernandez

Departamento de Biotecnología, Unidad de Química y Bioquímica, E.T.S. Ingenieros de Montes, Universidad Politécnica de Madrid, 28040 Madrid, Spain

ARTICLE INFO

Article history:
Received 2 March 2009
Received in revised form 13 April 2009
Accepted 15 April 2009
Available online 23 April 2009

Keywords:
Electron density
Electron localization function
Kinetic energy density
Electrostatic potential
Quantum calculations
Molecular properties

ABSTRACT

CheckDen, a program to compute quantum molecular properties on a variety of spatial grids is presented. The program reads as unique input wavefunction files written by standard quantum packages and calculates the electron density $\rho(\mathbf{r})$, promolecule and density difference function, gradient of $\rho(\mathbf{r})$, Laplacian of $\rho(\mathbf{r})$, information entropy, electrostatic potential, kinetic energy densities $G(\mathbf{r})$ and $K(\mathbf{r})$, electron localization function (ELF), and localized orbital locator (LOL) function. These properties can be calculated on a wide range of one-, two-, and three-dimensional grids that can be processed by widely used graphics programs to render high-resolution images. CheckDen offers also other options as extracting separate atom contributions to the property computed, converting grid output data into CUBE and OpenDX volumetric data formats, and perform arithmetic combinations with grid files in all the recognized formats.

1. Introduction

Current software for interactive visualization and analysis of three-dimensional maps and volumetric data is able to satisfy the stringent computational and algorithmic demands of molecular graphics. Joint developments in methods and techniques to render graphics along with the increasing power of computers are leading to a continuous advance in the capabilities of programs to analyze molecular structure and properties. The majority of these programs run on different operating systems and most of them are besides distributed free of charge in the Internet [1].

Molecular graphics software has been traditionally developed to display structures and properties (surfaces, electrostatic potentials, etc.) computed by the same program that renders the graphics. However, standard quantum packages do not include graphics capabilities and therefore the visualization of quantum results needs first convert their output into data files that might then be processed by graphics software [2]. These output data are typically limited to molecular orbitals, electron density, and electrostatic potentials. Furthermore, the underlying spatial mesh typically used for the graphical rendering of quantum properties lacks flexibility. CheckDen, the program presented in this paper, allows the user to define easily one-dimensional (1D), two-dimensional (2D), or three-dimensional (3D) arbitrary grids.

CheckDen is a standalone computer program written in Fortran90 that reads wavefunction wfn files outputted by standard quantum packages and creates a variety of data files that can be easily processed by widely used graphics programs. The current version of CheckDen is a greatly improved and extended version of one formerly reported in 2003 [3]. This program was initially intended to read information contained in *Check*point files created by earlier Gaussian [4] distributions and compute then some electron *Den*sity-dependent properties, which explains its name. The version presented here has been developed with the aim to provide a multipurpose tool to analyze results from quantum calculations and compute a variety of molecular properties.

CheckDen has the following useful features. (1) Apart from the electron density $\rho(\mathbf{r})$, it calculates a number of $\rho(\mathbf{r})$-dependent functions as the density difference function, the gradient and the Laplacian of $\rho(\mathbf{r})$, the information entropy, and the electrostatic potential. (2) The program computes also other functions as kinetic energy densities $G(\mathbf{r})$ and $K(\mathbf{r})$, the electron localization function, and the localized orbital locator function. (3) Atom contributions to the property computed can be optionally obtained and extracted to separate output files. (4) Any number of maximum and minimum property values with their spatial location can be determined. (5) All the functions can be computed at a variety of 1D, 2D, or 3D spatial grids easily defined in input. (6) Volumetric data for 3D grids can be optionally written in standard formats (Gaussian CUBE and

* Corresponding author. Tel.: +34 91 3364297; fax: +34 91 3366387.
E-mail addresses: luis.fpacios@upm.es (L.F. Pacios), afg@meteologica.es (A. Fernandez).

1093-3263/$ – see front matter © 2009 Elsevier Inc. All rights reserved.
doi:10.1016/j.jmgm.2009.04.008

OpenDX) which are recognized by the majority of molecular graphics programs available in the Internet. (7) CheckDen can be also used to perform simple arithmetic on different grid files to merge and combine volumetric data. (8) The program is open-source and well-known open-source Fortran90 compilers can be used to generate executable binaries on Windows and Linux distributions.

As illustrated in the examples reported below, some of these options allow us to obtain information from the wavefunction that is able to provide new insight into quantum properties of a molecular system. The rest of the paper is organized as follows. Section 2 presents a brief sketch of the functions computed in CheckDen while Section 3 describes succinctly the organization of the program and the spatial grids available. A number of illustrative examples are reported in Section 4 and finally, the distribution and installation of the program is summarily addressed in Section 5.

2. Methods

2.1. Input: form of the wavefunction

The main input to CheckDen is the wavefunction obtained in quantum calculations read from wfn files. These formatted plain-text files are created by Gaussian [4] and Gamess [5,6] packages and were popularized in computational chemistry as they were the main input to the former AIMPAC package [7]. wfn files have been maintained as input to updated programs dealing with applications from Atoms in Molecules (AIM) theory [8,9] as for example MORPHY [10], AIM2000 [11] and more recently, AIMAll [12]. TopMod [13], a package to perform topological analyses of the electron localization function (ELF) also uses wfn files as input.

The wavefunction is defined by N molecular orbitals $\varphi_i(\mathbf{r})$ (i = 1, 2, ..., N) (Kohn-Sham orbitals in DFT calculations) constructed as linear combinations of Gaussian basis functions

$$\varphi_i(\mathbf{r}) = \sum_{\mu=1}^{K} C_{\mu i}\chi_\mu \tag{1}$$

$$\chi_\mu(\mathbf{r}-\mathbf{R}_A) = \sum_{p=1}^{L} d_{p\mu} g_p(\alpha_{p\mu}, \mathbf{r}-\mathbf{R}_A) \tag{2}$$

where $d_{p\mu}$ are contraction coefficients of the expansion in primitive Cartesian Gaussians g_p

$$g_p = N_{p\mu}\, x_A^{l_x} y_A^{l_y} z_A^{l_z} \exp[-\alpha_{p\mu}(r-R_A)^2] \tag{3}$$

$N_{p\mu}$ is the normalization constant, exponents l_x, l_y, l_z define the angular type of the primitive (s: 0,0,0; x: 1,0,0; etc.), and $\alpha_{p\mu}$ is the orbital exponent of the Gaussian centered on nuclear position $\mathbf{R}_A$: $\{x_A, y_A, z_A\}$. wfn files give the molecular geometry, the specification of the set of Q primitives (Q values of (i) center assignments, (ii) Cartesian type codes, and (iii) orbital exponents), and M eigenvectors for the M molecular orbitals. Every eigenvector has Q coefficients for the expansion of molecular orbitals (1) in terms of (2), i.e., they include fixed contraction coefficients $d_{p\mu}$ and normalization factors $N_{p\mu}$ in (3).

2.2. Functions computed in CheckDen

CheckDen implements the calculation of the twelve functions listed in Table 1. Most of them are sufficiently well known in quantum chemistry and therefore only a brief account is next presented giving some references for more detailed explanations and illustrative applications.

Table 1
Functions computed in CheckDen.

Function	Symbol	Eq.
Electron density	$\rho(\mathbf{r})$	(6)
Promolecule density	$\rho^{\mathrm{pro}}(\mathbf{r})$	(7)
Density difference function	$\Delta\rho(\mathbf{r})$	(8)
Gradient of the density	$\bigtriangledown\rho(\mathbf{r})$	(9)
Magnitude of $\bigtriangledown\rho(\mathbf{r})$	$\lvert\bigtriangledown\rho(\mathbf{r})\rvert$	(10)
Laplacian of the density	$\bigtriangledown^2\rho(\mathbf{r})$	(11)
Kinetic energy density, G	$G(\mathbf{r})$	(16)
Kinetic energy density, K	$K(\mathbf{r})$	(17)
Electron localization function	$\eta(\mathbf{r})$	(18)
Information entropy	$S(\mathbf{r})$	(21)
Electrostatic potential	$V_{\mathrm{el}}(\mathbf{r})$	(22)
Localized orbital locator	$\gamma(\mathbf{r})$	(23)

2.2.1. Electron density

For a set of M occupied molecular orbitals with occupation numbers n_a (in closed shell systems, n_a = 2 and $M = N/2$), the electron density is

$$\rho(\mathbf{r}) = \sum_{a}^{M} n_a \varphi_a^*(\mathbf{r})\varphi_a(\mathbf{r}) \tag{4}$$

Defining the density matrix $P_{\mu\nu}$ as

$$P_{\mu\nu} = \sum_{a=1}^{M} n_a C_{\mu a}^* C_{\nu a} \tag{5}$$

the electron density takes the final form

$$\rho(\mathbf{r}) = \sum_{\mu}\sum_{\nu} P_{\mu\nu}\chi_\mu^*(\mathbf{r})\chi_\nu(\mathbf{r}) \tag{6}$$

Within the basis set of Q primitives used in wfn files, the essential information for an optimized molecular geometry is coded on the $Q \times Q$ density matrix P corresponding to the Cartesian Gaussians centered on nuclear locations $\{\mathbf{R}_A\}$.

2.2.2. Promolecule density

If $\rho^A(\mathbf{r})$ denotes the spherically averaged atomic density due to atom A located at the nuclear position $\mathbf{R}_A$ in the molecule, the promolecule density is defined by the sum

$$\rho^{\mathrm{pro}}(\mathbf{r}) = \sum_{A} \rho^A(\mathbf{r}) \tag{7}$$

Since it consists of overlapping spherical underformed atoms, is the default reference electron distribution for crystallographers. $\rho^{\mathrm{pro}}(\mathbf{r})$ has been extensively used to compute molecular surface properties [14] including large macromolecular structures [15] and to study charge distributions in molecular systems under the Hirshfeld stockholder partitioning of the electron density [16]. Note that for computing $\rho^{\mathrm{pro}}(\mathbf{r})$, one needs the atomic densities of isolated atoms obtained at the same level of theory as the molecule. To calculate (7), CheckDen needs thus to read atomic wfn files for the atom types present.

2.2.3. Density difference function (DDF)

The DDF is defined as the difference between the total electron density and the promolecule density:

$$\Delta\rho(\mathbf{r}) = \rho(\mathbf{r}) - \rho^{\mathrm{pro}}(\mathbf{r}) \tag{8}$$

This function is regarded as a deformation density associated to the redistribution of electron charge when the molecule forms from the constituting atoms. Regions where electron charge accumulates with respect to isolated atoms have positive $\Delta\rho(\mathbf{r})$ whereas regions of electron depletion have negative $\Delta\rho(\mathbf{r})$. The DDF has a long history [17] yet it continues being used in disparate contexts. The variation of $\Delta\rho(\mathbf{r})$ along selected directions has been

studied in formation of molecular systems in the framework of AIM theory [8,9] and still more recently, to propose new interpretations of several molecular properties [18].

2.2.4. Gradient of the density

`CheckDen` computes the gradient vector

$$\nabla\rho(\mathbf{r}) = \frac{\partial\rho}{\partial x}\mathbf{i} + \frac{\partial\rho}{\partial y}\mathbf{j} + \frac{\partial\rho}{\partial z}\mathbf{k} \tag{9}$$

giving the Cartesian components of vector (9) or alternatively its magnitude

$$|\nabla\rho(\mathbf{r})| = \left(\frac{\partial\rho}{\partial x}\right)^2 + \left(\frac{\partial\rho}{\partial y}\right)^2 + \left(\frac{\partial\rho}{\partial z}\right)^2 \tag{10}$$

at every point **r** for the spatial grid selected in input.

2.2.5. Laplacian of the density

The Laplacian of the electron density is

$$\nabla^2\rho(\mathbf{r}) = \frac{\partial^2\rho}{\partial x^2} + \frac{\partial^2\rho}{\partial y^2} + \frac{\partial^2\rho}{\partial z^2} \tag{11}$$

Since the Laplacian of a function at a point **r** gives the local curvature there, it measures the extent to which the function is locally concentrated or depleted at **r** with respect to points in the neighborhood. The use of the Laplacian of $\rho(\mathbf{r})$ in the AIM theory [8,9] as well as its relationship with the VSEPR model [19] are well known in current quantum chemistry. This function is being further explored in a variety of chemical applications [20].

2.2.6. Kinetic energy densities G(r) and K(r)

The characterization of interactions in terms of local contributions to the kinetic energy density was proposed in 1984 [21]. However, the *local* kinetic energy density is not uniquely defined. As a result from the application of the ∇^2 operator on the product $\Psi^*\Psi$

$$\nabla^2(\Psi^*\Psi) = \Psi^*\nabla^2\Psi + \Psi\nabla^2\Psi^* + 2\nabla\Psi^*\cdot\nabla\Psi \tag{12}$$

two local kinetic energy densities are defined as [8]:

$$G(\mathbf{r}) = \frac{1}{2}n\int \nabla\Psi^*\cdot\nabla\Psi\, d\boldsymbol{\tau} \tag{13}$$

$$K(\mathbf{r}) = -\frac{1}{4}n\int (\Psi^*\nabla^2\Psi + \Psi\nabla^2\Psi^*)d\boldsymbol{\tau} \tag{14}$$

If n is the number of electrons in the system, the $n\int d\boldsymbol{\tau}$ integration yields the one-electron property (here the kinetic energy) from the wavefunction Ψ. From Eq. (12) and recalling $\rho(\mathbf{r}) = n\int \Psi^*\Psi\, d\boldsymbol{\tau}$, the two forms (13) and (14) are related to each other as:

$$K(\mathbf{r}) = G(\mathbf{r}) - \frac{1}{4}\nabla^2\rho(\mathbf{r}) \tag{15}$$

Integrating this expression over *full space* yields the same value of the total kinetic energy T of the system, $K = G = T$, as the Laplacian integrates to zero. Recalling Eq. (6), kinetic energy densities (13) and (14) are computed in `CheckDen` in the form

$$G(\mathbf{r}) = \frac{1}{2}\sum_\mu\sum_\nu P_{\mu\nu}\nabla\chi^*_\mu(\mathbf{r})\cdot\nabla\chi_\nu(\mathbf{r}) \tag{16}$$

$$K(\mathbf{r}) = -\frac{1}{4}\sum_\mu\sum_\nu P_{\mu\nu}(\chi^*_\mu(\mathbf{r})\nabla^2\chi_\nu(\mathbf{r}) + \chi_\mu\nabla^2\chi^*_\nu) \tag{17}$$

Abramov proposed a method to obtain $G(\mathbf{r})$ from experimental electron densities [22] that was afterwards applied to theoretical $\rho(\mathbf{r})$ in hydrogen bond systems [23] and explored further to characterize bonding in crystal systems [24]. Local kinetic energy densities are extensively used to study interactions and bonding in a variety of systems [25–27].

2.2.7. Electron localization function (ELF)

This function, proposed initially by Becke and Edgecombe to measure electron localization in molecular systems [28], is defined as

$$\eta(\mathbf{r}) = \frac{1}{1 + [D(\mathbf{r})/D_h(\mathbf{r})]^2} \tag{18}$$

where $D(\mathbf{r})$ is an expression resulting from the probability density to find a same-spin electron and has the form [28]

$$D(\mathbf{r}) = \frac{1}{2}\sum_i |\nabla\varphi_i(\mathbf{r})|^2 - \frac{1}{8}\frac{|\nabla\rho(\mathbf{r})|^2}{\rho(\mathbf{r})} \tag{19}$$

The first term is the kinetic energy of the actual system made of fermions while the second term is the von Weizsäcker functional which gives the kinetic energy of a system made of particles without Pauli repulsion. Eq. (19) is thus interpreted as the excess kinetic energy density due to Pauli repulsion [29]. $D_h(\mathbf{r})$ in Eq. (18) is the reference Thomas–Fermi kinetic energy of a homogeneous electron gas of density $\rho(\mathbf{r})$, $D_h(\mathbf{r}) = c_F\rho(\mathbf{r})^{5/3}$ with $c_F = (3/10)(3\pi^2)^{2/3}$ (Fermi constant). Eq. (18) maps the ELF to the range [0,1]. High $\eta \to 1$ values indicate that electrons are more localized than in a uniform electron gas of the same density with $\eta = 1$ corresponding to a completely localized $D(\mathbf{r}) = 0$ situation. $\eta = 1/2$ means $D(\mathbf{r}) = D_h(\mathbf{r})$, i.e., the effect of Pauli repulsion is the same as in the homogeneous electron gas. Since $\rho(\mathbf{r})^{5/3}$ vanishes at large r much more rapidly than $D(\mathbf{r})$, $\eta \to 0$ when $r \to \infty$.

The number of applications that use the ELF to gain insight into chemical issues ranging from aromaticity to hydrogen bonding to reaction mechanisms has been continuously growing since 1991 when the first report of Savin et al. was published [29]. A topological methodology similar to AIM theory has been devised for the ELF [30] and a computer program (TopMod) to perform this topological analysis is available [13]. For updated examples and references on a variety of uses of the ELF, see [31–33].

2.2.8. Information entropy

Shanon proposed that the information entropy for a system with continuous probability $P(x)$ in one dimension could be characterized as [34]

$$S = -\int P(x)\ln P(x)dx, \qquad \int P(x)dx = 1 \tag{20}$$

which is a measure of the amount of information content of the underlying distribution. For chemical systems, one can define the Shanon entropy in position space, S_ρ, where the probability distribution is now the electron density $\rho(\mathbf{r})$:

$$S_\rho = \int S(\mathbf{r})d\mathbf{r} = -\int \rho(\mathbf{r})\ln\rho(\mathbf{r})d\mathbf{r} \tag{21}$$

The initial applications of this quantity in quantum chemistry [35,36] were subsequently widened to include studies on electron localization in chemical systems [37], molecular similarity [38,39], and measures of bond multiplicity [40]. The Shannon entropy continues being used in new ways to deal with information in atomic and molecular systems [41].

2.2.9. Electrostatic potential

The electrostatic potential V_{el} at **r** is expressed as

$$V_{el}(\mathbf{r}) = \sum_A \frac{Z_A}{|\mathbf{R}_A - \mathbf{r}|} - \int \frac{\rho(\mathbf{r}')}{|\mathbf{r} - \mathbf{r}'|}\, d\mathbf{r}' \tag{22}$$

It is created by the set of nuclei with nuclear charges Z_A located at $\mathbf{R}_A$ and the continuous electron density $\rho(\mathbf{r}')$. The value of V_{el} at $\mathbf{r}$ gives the energy acting on a probe point charge $q = +1$ located at $\mathbf{r}$ due to the net electrostatic effect resulting from positive point charges of nuclei and negative charge distribution of electrons. The sign of V_{el} indicates thus whether nuclei or electrons dominate at $\mathbf{r}$ and the product $\pm qV_{el}(\mathbf{r})$ is the electrostatic interaction energy between the molecule and the point charge. Ab initio electrostatic potentials have been extensively used in molecular reactivity and intermolecular interactions. The reader is referred to essential reviews by Politzer on chemical applications of electrostatic potentials [42–45]. For recent applications, see [45,46] and references therein.

2.2.10. Localized orbital locator (LOL)

This function was proposed by Schmider and Becke [47] to locate and characterize bond effects in terms of kinetic energy contributions. The LOL is defined as

$$\gamma(\mathbf{r}) = \frac{t(\mathbf{r})}{1 + t(\mathbf{r})}, \quad t(\mathbf{r}) = \frac{D_h(\mathbf{r})}{(1/2)\sum_i |\nabla\psi_i|^2} \tag{23}$$

The numerator of $t(\mathbf{r})$ is the kinetic energy of a homogeneous electron gas as in Eq. (18) and the denominator is the positive definite kinetic energy density. Because regions with high charge density (core regions) tend to dominate kinetic density, this term has little pronounced structural features. However, by comparing with a suitable reference value as $D_h(\mathbf{r})$, the features of bonding are made much more visible. The definition of $\gamma(\mathbf{r})$ in (23) is introduced just to map this quantity onto the finite range [0,1]. The LOL is thus a measure for the relative value of the local kinetic energy and due to the inverse relationship, it is larger for regions where the kinetic energy density is small (compared with the uniform electron gas). This function reveals localized electron locations without explicitly obtaining localized orbitals, hence its authors named it the localized orbital locator [47]. It has been shown [48] that $\gamma(\mathbf{r})$ is able to highlight chemically significant regions in atoms and molecules by identifying regions with small kinetic energy. The LOL has been also used to analyze experimental electron densities [49] and recently, its topology examined to characterize different bonds in transition metal complexes and hypervalent molecules [50].

3. Program

3.1. Initializing and input

Fig. 1 displays a flow chart of `CheckDen`. Upon initializing variables and setting internal data (van der Waals atomic radii, symmetry codes to organize basis sets, etc.), the program starts reading a text file named `CheckDen.input`. This file gives the options and input needed for setting the calculation (function and spatial grid selected, extra grid options, etc.) specified in a rather simple form using control parameters. The meaning of these parameters, their possible values and illustrative examples are detailed in a user manual included in the distribution (see Section 5). `CheckDen.input` also gives the name of the `wfn` file as well as a name used for the different output files created. The `wfn` file is then read to get the results from quantum calculations as indicated in Section 2.1 and the density matrix, Eq. (5), is computed.

3.2. Spatial grids available in `CheckDen`

The available spatial grids are listed in Table 2. Some "grids" are obviously not intended to perform actual mesh calculations. For instance, `KGrid` = 0 is just used to extract information from `wfn` files without actually doing any calculation. As explained below, `KGrid` = 13 and 14 process existing grid files to perform additional tasks. On the other side, two special 3D grids correspond to the set of nuclear positions (`KGrid` = 12) and N arbitrary points (`KGrid` = 11) with Cartesian coordinates given in the input stream (`CheckDen.input` file) or read from an external file. The rest of grids are four 1D, three 2D, and three 3D grids. The particular input defining every grid is entered according to the value of `KGrid` parameter (Table 2) as explained in the user manual. These grids cover a wide range of possibilities that give `CheckDen` a considerable flexibility to set spatial meshes to compute easily quantum properties.

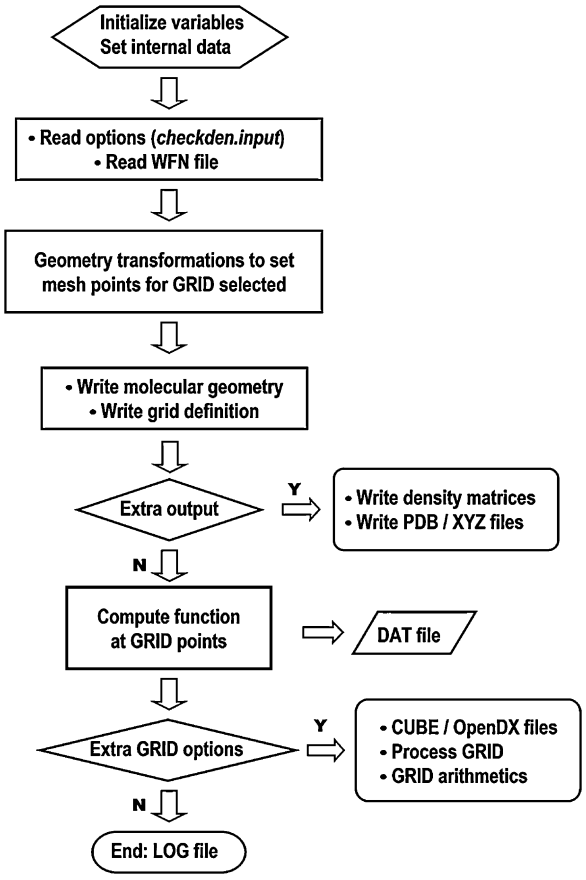

Fig. 1. Flow chart of `CheckDen` program.

Table 2
Space grids available in `CheckDen` by selecting the value of the `KGrid` parameter. *ND* is the number of space dimensions in the grid.

Grid type	`KGrid`	*ND*
No grid	0	–
Line parallel to *X*, *Y*, or *Z* axis	1	1
Line defined by two atoms	2	1
Bond line	3	1
Line defined by two arbitrary points	4	1
Plane *XY*, *XZ*, or *YZ* in the molecular frame	5	2
Plane defined by three atoms	6	2
Plane defined by three arbitrary points	7	2
3D Box-VdW	8	3
3D Cartesian box	9	3
3D Scaled Box-Mol	10	3
N arbitrary space points	11	3
Nuclear positions	12	3
Read an existing `Grid` file	13	–
Do arithmetic with `Grid/DX/Cube` files	14	–

3.3. Output

The program creates a LOG file where basic information on the molecular system as well as parameters defining the selected function and spatial grid are recorded. After performing the geometry transformations needed to set mesh points in the molecular system, CheckDen writes in this LOG file the molecular geometry, dimensions of the system and definition of the grid in the molecular frame. Optionally, the program writes separate molecular geometry files in XYZ or PDB formats and includes formatted density matrices (either for the molecule or for separate components in the DDF) in the LOG file.

The main output of the calculation is recorded in a formatted DAT file that gives the set of grid points and values of the function obtained as explained in the next subsection. A particularly useful option is the possibility to include atomic contributions from all the atoms in the molecular system to the function value at every grid point. This feature allows to extract then particular contributions from selected atoms to separate grid files, either at the same run or at a later KGrid = 13 run.

3.4. Calculation of the selected function

The selected function is calculated in MakeGrid, a subroutine which is essentially a large SelectCase construct whose Case blocks compute the different functions in Table 1. Every function Case is in turn organized in two alternative code segments dubbed *Special* and *General* grid blocks. *Special* grids either require parameters defined by a geometry transformation (KGrid = 2, 3, 4, 6, and 7) or they are composed of arbitrary points (KGrid = 11 and 12). *General* grids are built starting at an initial (x_0, y_0, z_0) point as $x_i = x_{i-1} + \Delta x$, $y_i = y_{i-1} + \Delta y$, $z_i = z_{i-1} + \Delta z$ and both x_0, y_0, z_0 values and Δx, Δy, Δz stepsizes are defined in the molecular frame (KGrid = 5, 8, 9, and 10). Both *Special* and *General* code blocks are made of $(x, (y, (z)))$ dimension loops posed by the particular selected grid and a subroutine is called in the innermost loop to calculate the primitive Gaussians at (x_i, y_i, z_i). If the function needs first or second partial derivatives, a subroutine which codes the closed analytical forms of these derivatives for every Cartesian type is called. Electrostatic potentials need to evaluate one-electron integrals between pairs of primitive functions arising from the electron term in Eq. (22). This is performed by several routines that code the closed analytical form of these integrals in terms of power expansion series in Cartesian components of the integrand defined by l_x, l_y, l_z exponents in Eq. (3).

As far as the program works over the set of primitive Gaussians centered on atoms, all the calculations are organized so as to keep record of values arising from each atom. If selected in CheckDen.input, these atom contributions can optionally be outputted to the DAT file. Of course, functions that need the local value of the total $\rho(\mathbf{r})$ (magnitude of $\bigtriangledown\rho(\mathbf{r})$, Shanon information entropy, ELF, and LOL) are excepted from this possibility.

3.5. Additional grid options available in CheckDen

The options exists to convert 3D volumetric data into OpenDX or Gaussian CUBE formats that are recognized by most of the molecular graphics programs available. OpenDX stands for *Open Data eXplorer*, formerly *IBM Data Explorer*, and now open source (www.opendx.org). It is a powerful standard for 3D visualization that can represent quantities color coded. OpenDX software can make cuts in the object to have views of the inside, rotate the object to have a view from any angle and make animations of these movements. These representations may use a great variety of options to render graphics of the highest quality. CUBE files are plain-text files created by Gaussian package to store volumetric elements at a 3D grid defined at the header section. CUBE files are similar to OpenDX files in that both store data on a voxel element basis. They differ in that CUBE files include atom positions and can besides incorporate the gradient of the density giving three values per point instead the unique value per point of any other scalar property. There are several free molecular graphics programs that recognize OpenDX and CUBE files as for instance, *Chimera* [51], *Jmol* [52], *PyMOL* [53], and *VMD* [54]. It is thus possible to render easily 3D high-quality pictures of ab initio properties computed with CheckDen.

The program offers also a number of additional options to post-process grid data files (either computed at the same run or created in previous runs). These include the option to truncate property values, locate either number of maxima and minima, and extract selected atom contributions from existing grid data files to separate files. KGrid = 13 is used to read existing files containing grid data from previous runs and perform these additional tasks. On the other side, a KGrid = 14 run asks to do simple arithmetic with existing grid files in all the recognized formats to combine and merge grid data previously computed.

3.6. Other features of CheckDen

The program is organized to avoid code biffurcations (use of If's) as much as possible by defining separate blocks as discussed above. After rewriting a good part of the code, the current version of CheckDen is considerably faster than the preceding version [3]. However, the speedup obtained by compiling the code activating optimization for faster execution is usually dramatic (see Section 5).

4. Application examples

We present in this section a selection of examples involving different functions and spatial grids intended to illustrate the capabilities of CheckDen. These examples refer to the following molecular systems: ClO–H_2O hydrogen bond complex, acetic acid molecule, and three conformations of biphenyl.

4.1. DDF profiles along interatomic lines

Fig. 2 displays profiles of the DDF along lines defined by Cl–O_1 and H_1–O_2 bonds in the ClO–H_2O complex at the MP2/aug-cc-pVTZ geometry shown at the top. Profiles in the complex are compared with those of isolated ClO and H_2O monomers optimized at the same level of theory. The DDF is computed at 301 points with 0.025 Å stepsize along lines defined by two atoms (KGrid = 2, Table 2) starting at 3.0 Å from the first atom. The DDF is first computed on the complex and then on isolated ClO and water monomers. The four 1D grid files are finally plotted with *Gnuplot 4.2.4* [55].

Negative values of this function defined in Eq. (8) mean that the total electron density is greater in the separate non-interacting atoms than in the molecule. In other words, if the DDF is negative at a point, there is no accumulation of electron charge facilitating bonding at this point. Fig. 2 shows that electron density is depleted along the HO line rather similarly in water and in the complex. On the contrary, ClO bond exhibits a rather different behavior suggesting that Cl and O atoms favor bonding in chlorine monoxide monomer (positive DDF) yet not so in the complex.

4.2. Contour maps of kinetic energy density G(r)

Fig. 3 shows contour maps of kinetic energy density $G(\mathbf{r})$ at the plane containing all the atoms in ClO–H_2O complex (top) and the difference between $G(\mathbf{r})$ in the complex and in both non-

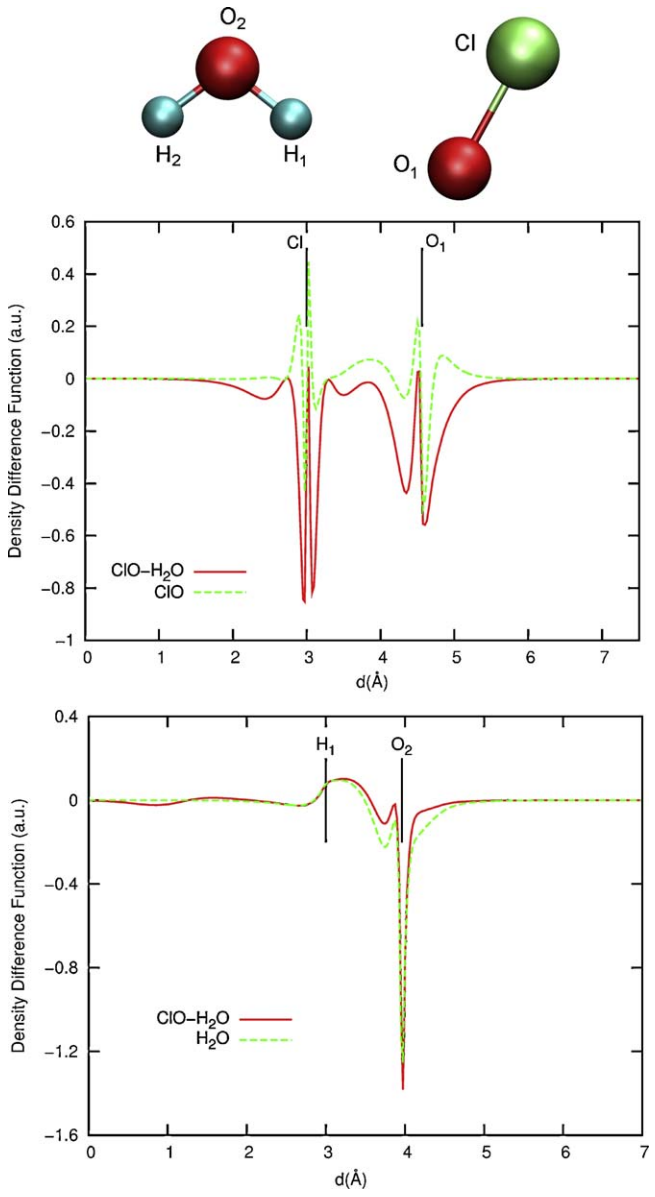

Fig. 2. Top: MP2/aug-cc-pVTZ optimized geometry of ClO–H_2O complex. Plots: profile of the DDF along a line defined by Cl–O_1 bond in the complex and in the isolated ClO monomer (upper) and along a line defined by H_1–O_2 bond in the complex and in isolated water (lower). Vertical black lines indicate atom positions at the lines in the complex.

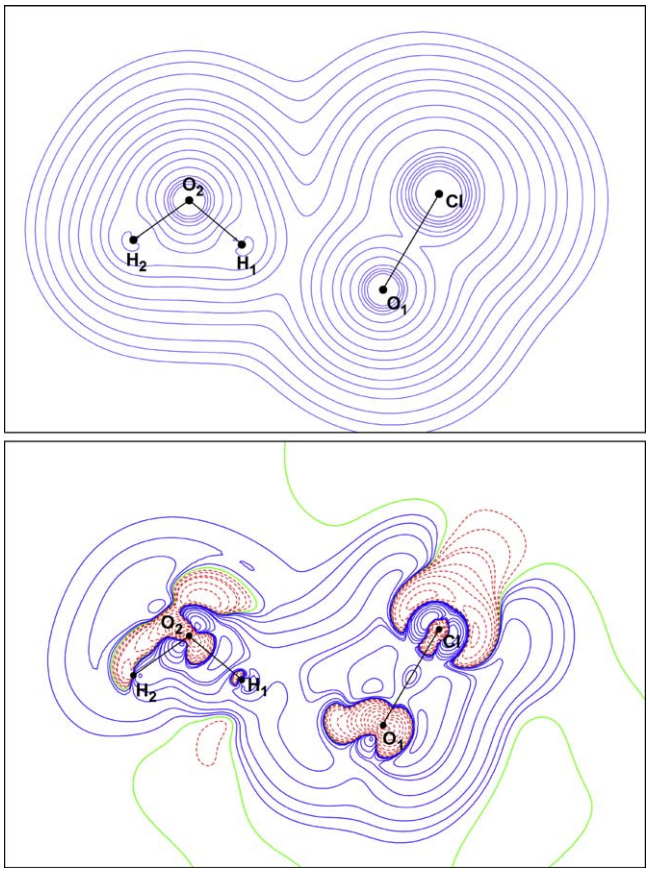

Fig. 3. Top: contours map of kinetic energy density $G(\mathbf{r})$ at the plane of ClO–H_2O complex. Contour levels are $2^m \times 10^n$, with $m = 1, 2, 3$ for every n of set $n = -4, -3, -2, -1, 0$ increasing innerwards. Bottom: contours map of the difference between $G(\mathbf{r})$ in the complex and separate $G(\mathbf{r})$ in both monomers at the complex geometry. Contour 0 is colored green while blue and red are positive and negative, respectively, $2^m \times 10^n$ contours with $m = 1, 2, 3$ for every n of set $n = -5, -4, -3, -2, -1, 0, 1$.

interacting monomers placed at the complex geometry (bottom). While the first map illustrates the actual distribution of kinetic energy density in the complex, the second map aims to describe changes of monomer kinetic densities upon complex formation. Since all the atoms lie at a plane (*XY* in the molecular frame), the grid selected is a 2D *XY* plane at $Z = 0$ (`KGrid` = 5, Table 2) and $G(\mathbf{r})$ is computed at $181 \times 121 = 21{,}901$ points with 0.05 Å stepsize in both directions (top). After having calculated this function (1) at the complex, it is computed separately using the same grid in (2) ClO and (3) H_2O monomers *at the complex geometry*. These three grid files are then combined in a `KGrid` = 14 run to obtain the difference map as (1)–(2)–(3) (bottom). Maps in Fig. 3 were plotted with *Surfer 8* (Golden Software Inc., Golden (CO), 2002, www.goldensoftware.com).

Except that kinetic energy density raises rapidly near the nuclei (the highest contour plotted is 8.0 a.u.) and that the magnitude of $G(\mathbf{r})$ embracing the interacting monomers is considerable (the first broken contour plotted is 0.02 a.u.), the map of $G(\mathbf{r})$ is featureless. On the contrary, the difference map provides detailed views on regions where electrons move faster or slower upon complex formation. Note how atoms in the O_2–$H_1 \cdots O_1$ H-bond exhibit inner regions of negative contours (i.e., lower kinetic energy in the complex). Oxygens show distorded regions that suggest a kind of "polarization" in the hydrogen bond direction contrarily to that noticed in chlorine which exhibits symmetric changes with negative areas extending outer far and is consistent with a much smaller participation of this atom in the interaction. Although positive contours dominate the inter-monomer region, they locally decrease in the vicinity of H_1 (directly involved in hydrogen bonding)

4.3. 2D and 3D plots of electrostatic potentials

Electrostatic potential plots of the ClO–H_2O complex are displayed in Fig. 4. Contours map (top) corresponds to the *XY* plane at $Z = 0.0$ (`KGrid` = 5, Table 2) with $V(\mathbf{r})$ computed at $91 \times 61 = 5551$ points and 0.1 Å stepsize in both directions. This map was plotted with *Surfer 8*. It must be stressed that although this system has only 5 atoms, the level of theory used gives rise to 193 molecular orbitals and 341 primitive Gaussians. The different computational effort involved in calculating $V(\mathbf{r})$ and any other function is illustrated by comparing the CPU time needed to obtain this map (5551 points), 69 s on a 2Quad Intel, 2.40 GHz, RAM 2Gb PC, with the CPU time to obtain the first map of $G(\mathbf{r})$ in Fig. 3 (21,901 points), 17 s.

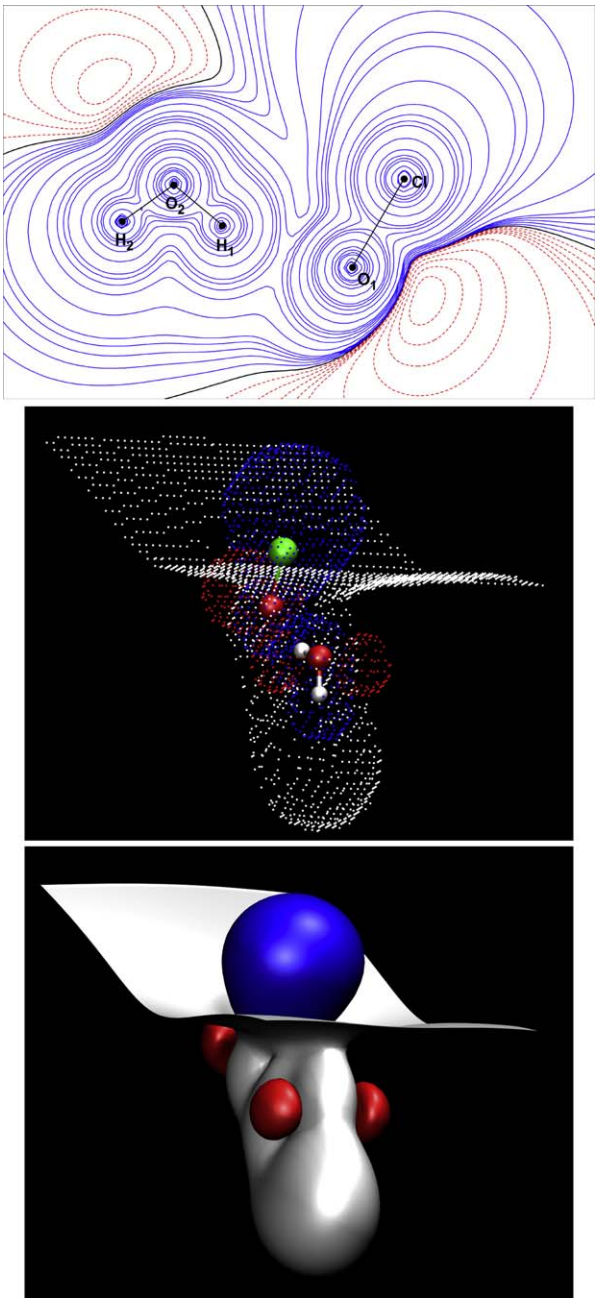

Fig. 4. Top: contours map of the electrostatic potential $V(\mathbf{r})$ at the plane of ClO–H_2O complex. Black contour is $V(\mathbf{r}) = 0.0$, negative contours (red dot lines) span the range (−0.002 to −1.0) a.u., and positive contours (blue solid lines) span the range (+0.002 to +60.0) a.u. Middle: 3D plot of three spatial isocontours of $V(\mathbf{r})$ around the complex, 0.0 (white), −0.04 (red), and +0.04 (blue) a.u., depicted as dot isosurfaces. The structure of ClO–H_2O shown inside 0.0 isosurface is a perspective view of the geometry drawn in Fig. 2. Bottom: same plot rendered with solid isosurfaces.

3D plots in Fig. 4 were obtained by computing $V(\mathbf{r})$ at 71 × 51 × 41 = 148,461 points with 0.2 Å stepsize in each direction at a Cartesian box grid (`KGrid` = 9, Table 2). Grid data file was then converted into `CUBE` volumetric format and rendered with *VMD 1.8.6* [54]. ±0.04 a.u. isosurfaces correspond to a potential energy about 25 kcal mol^{-1}.

This complex shows an electrostatic feature characteristic of moderate hydrogen bonding, namely, the division of space into negative and positive regions so that the electropositive domain encloses the whole system [46,56]. Due to the opposite electrostatic nature of H-donors and H-acceptors, H-bond formation can be regarded as the consequence of a complementarity between interacting monomers [46,56]. The net positive potential embracing the H-bond system highlights the dominant electrostatic role played by hydrogen in this interaction [46]. As for Fig. 4, it is interesting to note how the $V(\mathbf{r}) = 0$ isocontour traces out a bag-shaped surface that encloses the whole complex and how despite the same magnitude of both non-zero 3D isosurfaces (0.04 a.u.), they exhibit rather different shapes. Negative $V(\mathbf{r})$ is confined to small volumes at both sides of oxygen in water and behind this atom in the ClO moiety, suggesting thus electrostatic effects arisen from lone pairs. Positive $V(\mathbf{r})$ occupies a large volume around Cl atom that extends far outside the complex and reveals a direction in space for nucleophile attack, indeed one of the main issues of interest in analyses of electrostatic potentials [42–44,56].

4.4. Spatial distributions of the LOL function

Examples on the ClO–H_2O complex are completed with two views of the spatial distribution of the LOL function $\gamma(\mathbf{r})$ in Fig. 5. To obtain these plots, $\gamma(\mathbf{r})$ was calculated at 121 × 81 × 61 = 597,861 points with 0.1 Å stepsize in each direction at a Cartesian box grid (`KGrid` = 9). The grid data file was then converted into `OpenDX` volumetric format and rendered with *Jmol 11.6.3* [52]. Because this function is confined to the finite range [0,1], 0.55 and 0.70 isocontours in Fig. 5 represent regions of high electron localization whereas the lowest localization is represented by the 0.10 isocontour in these plots. If $t(\mathbf{r}) = D_h(\mathbf{r})$ in Eq. (23), $\gamma(\mathbf{r}) = 1/2$ and electrons have the same kinetic energy as the homogeneous electron gas model reference. $\gamma(\mathbf{r}) = 0.50$ surface is thus the boundary that separates "slow" ($\gamma(\mathbf{r}) > 1/2$) from "fast" ($\gamma(\mathbf{r}) < 1/2$) regions. Covalent bonds manifest as local LOL maxima [47–49], a result in accordance with the fact that the local kinetic energy is lowered in a covalent bond [8,47]. In hydrogen, where no core exists, the nucleus is within the slow bond region. Apart from bonds, $\gamma(\mathbf{r}) > 1/2$ also occurs in regions associated with electron lone pairs.

All these features are nicely illustrated in Fig. 5, where higher LOL regions in the plane slice (orange-red isocontours) clearly map covalent bonds as well as cuts of lone pairs regions. Inner surfaces in the 3D plot (yellow) are still clearer in illustrating not only the slow regions along covalent bonds but more dramatically, lone pairs domains around oxygen and chlorine atoms.

4.5. Maps of electron density and its Laplacian

Plots of $\rho(\mathbf{r})$ and $\nabla^2\rho(\mathbf{r})$ in the carboxyl plane in acetic acid at a MP2/6-311G(d,p) geometry are shown in Fig. 6. The electron density was calculated at 41 × 41 × 41 = 68,921 points with 0.2 Å stepsize in each direction at a Cartesian box (`KGrid` = 9), the grid data file converted into `OpenDX` format and rendered with *Jmol 11.6.3* [52]. To obtain $\nabla^2\rho(\mathbf{r})$ map, the Laplacian was calculated at 321 × 321 = 103,041 points with 0.025 Å stepsize in both directions at the *XZ* plane at $Y = 0$ (`KGrid` = 5) and the map plotted with *Surfer 8*. Fig. 6 involves two rather different resolutions to convey information on the electron distribution. While the rough mesh of $\rho(\mathbf{r})$ illustrates how a proper isocontour (0.40 a.u.) traces out the molecular skeleton, the fine mesh of $\nabla^2\rho(\mathbf{r})$ gives a detailed view of domains where electron charge accumulates (negative contours) or depletes (positive contours).

4.6. Contours maps of electron density differences

The capabilities of `CheckDen` to combine grid data and extract atom contributions make it a useful tool to analyze changes of ab initio properties related with processes as complex formation (preceding examples) or internal rotation (deal with hereafter) to

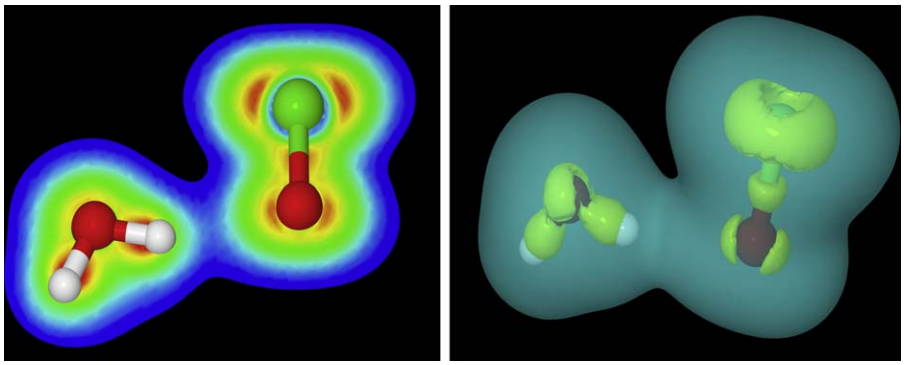

Fig. 5. Spatial distribution of the LOL function $\gamma(\mathbf{r})$ in ClO–H_2O complex. Left: slice on the plane containing the atoms. Isocontours are color coded in a continuous color scheme between blue for the outermost contour (0.10) and red for the highest contour (0.70). Right: 3D plot of two isocontours of $\gamma(\mathbf{r})$ around the complex, 0.10 (translucent outer isosurface in cyan) and 0.55 (solid inner isosurface in yellow).

quote just two relevant instances. We address now differences between electron densities of biphenyl conformations given by the torsional angle between phenyl rings, ϕ. B3LYP/6-311G(d,p) calculations predict an equilibrium geometry with a twisted conformation for $\phi = 40.5^\circ$ (shown at the top of Fig. 7) in good agreement with experiment and higher levels of theory [57]. Two additional geometries were also optimized at the B3LYP/6-311G(d,p) level without symmetry constraints except fixing ϕ at 0° and 90° to obtain plane and perpendicular conformations, respectively.

Fig. 7 shows contours maps of the following differences between electron densities of biphenyl conformations: 0°–ϕ_{min}, ϕ_{min}–90°, and 0–90°. To obtain these maps, $\rho(\mathbf{r})$ was first calculated at $121 \times 151 = 18{,}271$ points with 0.1 Å stepsize in both directions at the plane of the phenyl ring bearing H_1, C_1, and H_3 atoms (Fig. 7, top). This calculation was carried out for $\phi = 0^\circ$, ϕ_{min}, and $\phi = 90^\circ$ geometries and these grid files combined in three `KGrid` = 14 runs to obtain differences data files plotted in Fig. 7 (with *Surfer 8*). These maps show therefore electron shifts occurring at a phenyl ring upon rotation of the other ring. As recalled in [32], discussions on the origin of the rotational barrier of biphenyl in terms of a balance between steric repulsion effects suffered by hydrogens in *ortho* and electron conjugation effects in phenyl rings have a long and lively story. Maps in Fig. 7 are in accordance with that one might expect from loss of conjugation when conformation apart from planarity. These maps show alternating regions where $\rho(\mathbf{r})$ increases and decreases inside the "static" ring. They agree also in describing depletion of electron density around *ortho* positions and along *meta* positions (blue contours). 0°–ϕ_{min} and 0–90° maps are nearly identical, which indicates that once planarity is lost, it makes little difference whether the other ring is at 40.5° or 90°. Upon internal rotation, $\rho(\mathbf{r})$ around inter-ring C_1–C_2 bond decreases in both maps whereas the opposite happens in ϕ_{min}–90°. In other words, the inter-ring bond has a greater electron density in the ϕ_{min} conformation, an interesting result insofar as a point in the controversy on this rotational barrier regards the strengthening of this bond as a crucial feature (see the overview in Ref. [32]).

4.7. 3D plots of electron density differences

Fig. 8 displays two 3D isosurfaces of the differences represented in Fig. 7. To obtain these plots, $\rho(\mathbf{r})$ was first calculated at $81 \times 81 \times 131 = 859{,}491$ points with 0.1 Å stepsize in every direction at a Cartesian box (`KGrid` = 9) for $\phi = 0^\circ$, ϕ_{min}, and $\phi = 90^\circ$ geometries of biphenyl. These grid files were then converted into `OpenDX` format, combined in three `KGrid` = 14 runs to obtain volumetric data files for $\rho(\mathbf{r})$-differences, and rendered with *VMD* 1.8.6 [54]. Fig. 9 shows a complementary view to highlight the spatial redistribution of electron density occurring on the "static" phenyl ring upon rotation of the other ring. This plot corresponds to the 0–90° `OpenDX` file and was rendered with *PyMOL 1.1* [53].

Although much larger volumes of alternating sign in these $\rho(\mathbf{r})$-differences are obviously associated to the rotating phenyl, Figs. 8 and 9 show that the "static" ring feels significant effects. At the

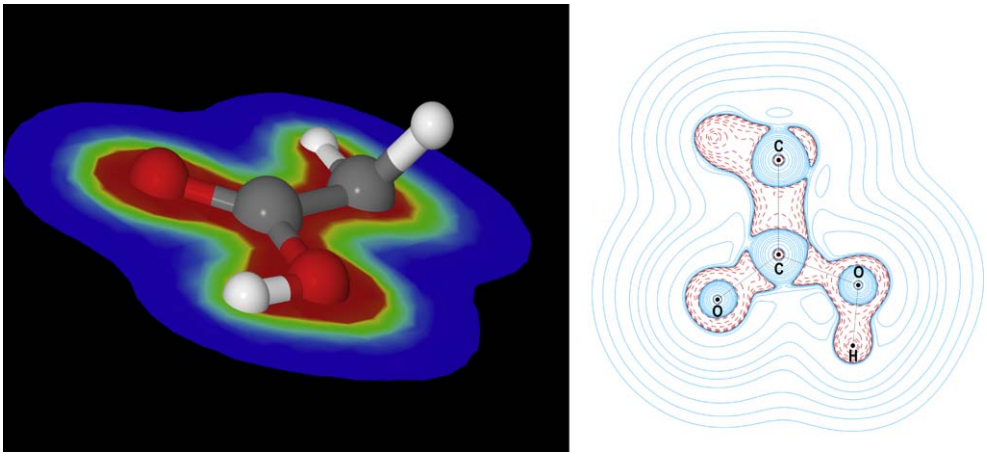

Fig. 6. Left: slice on the carboxyl plane in acetic acid of electron density $\rho(\mathbf{r})$ isocontours color coded with a continuous color scheme between blue for the outermost contour (0.001 a.u.) and red for the highest contour (0.40 a.u.). Right: isocontours map of the Laplacian of $\rho(\mathbf{r})$ at the carboxyl plane. Contour 0 is colored black while solid blue and dashed red are positive and negative, respectively, $2^m \times 10^n$ a.u. contours with $m = 1, 2, 3$ for every n of set $n = -3, -2, -1, 0, 1, 2$.

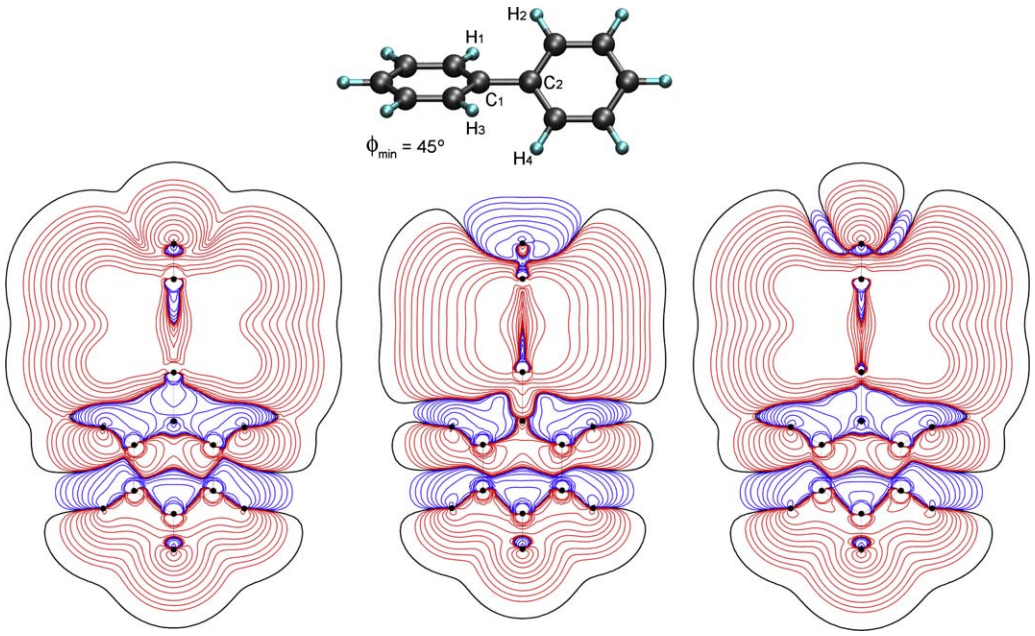

Fig. 7. Top: B3LYP/6-311G(d,p) optimized geometry of biphenyl. Contours maps: difference between electron densities of two conformations of biphenyl given by the dihedral ϕ (H_1–C_1–C_2–H_2) plotted at the plane of the phenyl ring assumed to remain static upon internal rotation (bottom in maps). Differences from left to right: 0°–ϕ_{min}, ϕ_{min}–90°, and 0–90°. Black contour is 10^{-6} a.u. while red and blue are positive and negative, respectively, $2^m \times 10^n$ a.u. contours with m = 0, 1, 2 for every n of set n = −5, −4, −3, −2.

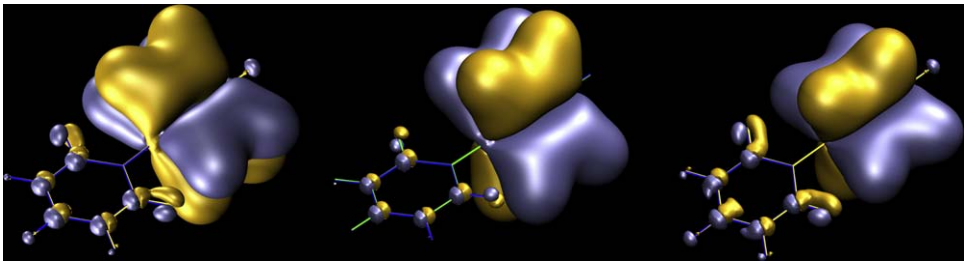

Fig. 8. Two 3D isosurfaces, −0.01 a.u. (yellow) and +0.01 a.u. (blue), of the difference between electron densities of two conformations of biphenyl. From left to right: 0°–ϕ_{min}, ϕ_{min}–90°, and 0–90°. Right phenyl ring rotates respect to the left phenyl ring.

relatively large values of $\rho(\mathbf{r})$-differences considered in Fig. 8 and still more clearly at the isosurface values drawn in Fig. 9, these plots show that there is a decrease of electron density in the region inside ring of carbons in *meta* and, to a greater extent, in the region

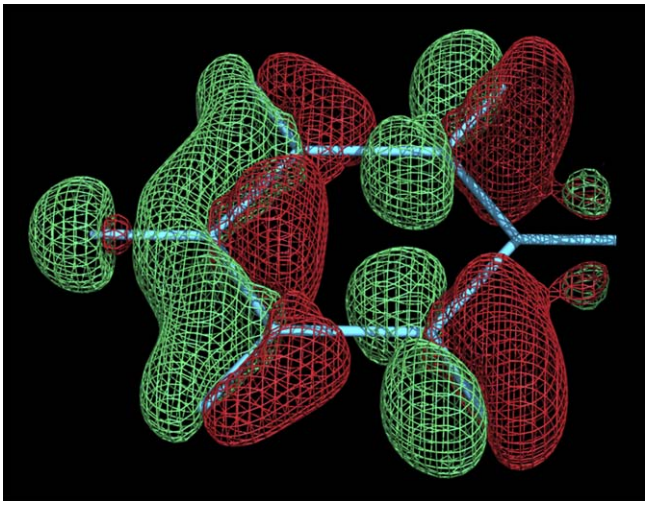

Fig. 9. Two wireframe 3D isosurfaces, −0.003 a.u. (red) and +0.003 a.u. (green), of the difference between electron densities of ϕ = 0° and 90° conformations of biphenyl at the phenyl ring assumed to remain static upon internal rotation.

that points towards the other phenyl of atoms in *ortho*. This effect, already noticed in Fig. 7, indicates that upon internal rotation and besides lowering of possible steric repulsion between hydrogens in *ortho*, electron charge is depleted from the region between rings when biphenyl apart from planarity. This is a reasonable result if one considers that a planar structure might favor the sharing of electron density between rings.

4.8. 3D plots of atom contributions to electron density differences

This last biphenyl example illustrates contributions from particular atoms to changes occurring on electron density upon internal rotation. Fig. 10 shows contributions arising from bonded C_1 and C_2 atoms as well as opposite H_1 and H_2 atoms in *ortho* (see Fig. 7, top) to the 0–90° $\rho(\mathbf{r})$-differences between planar and perpendicular conformations. Fig. 10 was prepared as follows. First, $\rho(\mathbf{r})$ was calculated at 61 × 61 × 111 = 413,031 points with 0.1 Å stepsize at a Cartesian box (`KGrid` = 9) generating grid files that include contributions from all the atoms for both ϕ = 0° and 90° geometries of biphenyl. Secondly, two `KGrid` = 13 runs were performed to extract the contributions from C_1, C_2, H_1, and H_2 atoms to separate `OpenDX` files. Thirdly, these files were combined in `KGrid` = 14 runs to create volumetric data files that were rendered with *PyMOL 1.1* [53] to obtain Fig. 10.

To analyze Fig. 10 bear in mind that positive isosurfaces indicate that $\rho(\mathbf{r})$ in ϕ = 0° conformation is greater than in ϕ = 90°

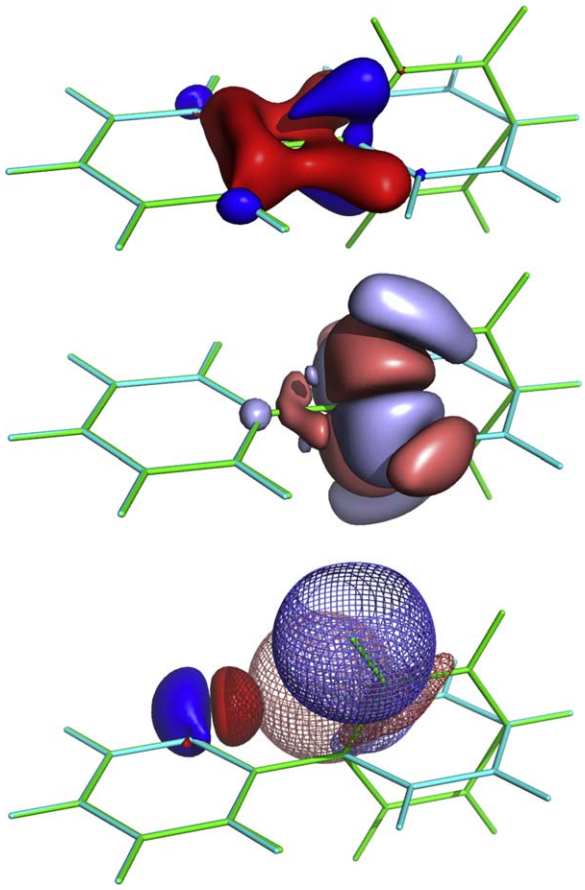

Fig. 10. Two isosurfaces, −0.0015 a.u. (red and salmon) and +0.0015 a.u. (blue and light blue), of the difference between the following atom contributions to electron densities of $\phi = 0^\circ$ (cyan framework) and $\phi = 90^\circ$ (green framework) conformations of biphenyl. Top: C_1. Middle: C_2. Bottom: H_1 and H_2 (for atom labels, see the biphenyl structure drawn in Fig. 7).

and conversely for negative isosurfaces. Since C_1 is in the "static" phenyl while C_2 is in the rotating phenyl, the former must loose net density when conformation changes from planar to perpendicular while the latter must gain it. However, note the rather different shapes associated to these variations and how the effect arising from C_1 affect C_2 to a much greater extent than the converse effect. This behavior is in sharp contrast with that exhibited by both hydrogens in *ortho*. The $\rho(\mathbf{r})$-difference on H_1 atom in the "static" phenyl is positive along H_1–C bond and negative in the inter-ring region (blue and red solid surfaces, respectively, in bottom plot) while the $\rho(\mathbf{r})$-difference on H_2 shows large spherical regions with greater electron density in the conformation with less steric hindrance between H_2 and H_1 (wireframe surfaces in bottom plot).

Further detailed analyses of maps and 3D plots like those presented here would be useful in exploring the subtle electron redistribution effects associated to internal rotation. The study of changes in the explored function ($\rho(\mathbf{r})$ or any other in Table 1) occurring on the molecule as a whole or on particular atom contributions upon internal rotation should be useful to explore variations of interatomic interactions from a new viewpoint. This should provide information of interest on current discussions regarding the ultimate nature of internal rotation. In either event, such studies had to be the subject of further specific reports. Our aim in selecting here this topic was just presenting an example of the capabilities of `CheckDen` as a powerful tool to analyze quantum properties.

5. Distribution and installation of `CheckDen`

The program is freely available at the URL http://atenea.montes.upm.es. Two versions with precompiled binaries for Linux (x86_64 openSUSE 11.0) and Windows platforms are provided. The source Fortran90 code file as well as a complete user manual and input examples are included in the distribution of `CheckDen`.

In the event that the source had to be compiled to get suited binaries (because either one uses other Linux distributions or some changes to the code are made), existing open-source Fortran compilers can be employed. In this regard, we have successfully tested two particular well-known free compilers: *G95* (www.g95.org) for Windows and *gfortran* (www.gfortran.org) for Linux. However, it is strongly recommended to check the compiler documentation to optimization options in order to generate faster executables: speedup obtained this way can be dramatic as the following example illustrates. Computing the electron density at a plane grid of 241 × 361 = 77,361 points on a certain molecular system took 24 s CPU under Windows (32-bit) and 19 s under Linux (64-bit) using executables built up without optimization with *G95* and *gfortran*, respectively. Including proper optimization options, these times on the same problem were decreased to 7 and 4 s, respectively!

Acknowledgement

Financial support from Comunidad de Madrid, Spain, under contract/grant number S-0505/AMB/029 is gratefully acknowledged.

References

[1] The *Molecular Graphics* link in the *Software* block of *General Information/External Links* entry in the Protein Data Bank webpage (www.pdb.org) gives a useful updated list of commented links to widely used molecular graphics programs.
[2] The *Linux4Chemistry* webpage (www.redbrick.dcu.ie/~noel/linux4chemistry/) maintains a useful list of commented links to programs accessible by category (3D Viewer, Molecular Dynamics, Quantum Mechanics, ...).
[3] L.F. Pacios, CheckDen: a computer program to generate 1D, 2D, and 3D grids of functions dependent on the molecular ab initio electron density, Comput. Biol. Chem. 27 (2003) 197–209.
[4] M.J. Frisch, et al., Gaussian 03, Revision C.02, Gaussian, Inc., Wallingford, CT, 2004
[5] M.W. Schmidt, K.K. Baldridge, J.A. Boatz, S.T. Elbert, M.S. Gordon, J.H. Jensen, S. Koseki, N. Matsunaga, K.A. Nguyen, S.J. Su, T.L. Windus, M. Dupuis, J.A. Montgomery, General atomic and molecular electronic structure system, J. Comput. Chem. 14 (1993) 1347–1363.
[6] M.S. Gordon, Advances in electronic structure theory: GAMESS a decade later, in: C.E. Dykstra, G. Frenking, K.S. Kim, G.E. Scuseria (Eds.), Theory and Applications of Computational Chemistry, the First Forty Years, Elsevier, Amsterdam, 2005, pp. 1167–1189.
[7] F.W. Biegler-König, R.F.W. Bader, T.H. Tang, Calculation of the average properties of atoms in molecules, J. Comput. Chem. 13 (1982) 317–328.
[8] R.F.W. Bader, Atoms in Molecules. A Quantum Theory, Oxford University Press, Oxford, 1990.
[9] P.L. Popelier, Atoms in Molecules: An Introduction, Prentice Hall, London, 2000.
[10] P.L. Popelier, MORPHY, a program for an automated "atoms in molecules" analysis, Comput. Phys. Commun. 93 (1996) 212–240.
[11] F.W. Biegler-König, J. Schönbohm, D. Bayles, AIM2000—a program to analyze and visualize atoms in molecules, J. Comput. Chem. 22 (2001) 545–559.
[12] AIMAll (Version 08.10.29), Todd A. Keith, 2008 (aim.tkgristmill.com).
[13] S. Noury, X. Krokidis, F. Fuster, B. Silvi, Computational tools for the electron localization function topological analysis, Comput. Chem. 23 (1999) 597–604.
[14] A.S. Mitchell, M.A. Spackman, Molecular surfaces from the promolecule: a comparison with Hartree-Fock ab initio electron density surfaces, J. Comput. Chem. 21 (2000) 933–942.
[15] X. Girones, L. Amat, R. Carbó-Dorca, Modeling large macromolecular structures using promolecular densities, J. Chem. Inf. Comput. Sci. 42 (2002) 847–852.
[16] F. De Proft, C. Van Alsenoy, A. Peeters, W. Langenaeker, P. Geerlings, Atomic charges, dipole moments, and Fukui functions using the Hirshfeld partitioning of the electron density, J. Comput. Chem. 23 (2002) 1198–1209.
[17] E. Steiner, Density-difference maps in quantum chemistry, Theor. Chem. Acc. 60 (1982) 561–572.
[18] J.F. Harrison, On the role of the electron density difference in the interpretation of molecular properties, J. Chem. Phys. 119 (2003) 8763–8764.
[19] R.J. Gillespie, P.L.A. Popelier, Chemical Bonding and Molecular Geometry. From Lewis to Electron Densities, Oxford University Press, New York, 2001.

[20] C.F. Matta, R.J. Boyd (Eds.), The Quantum Theory of Atoms in Molecules, Wiley-VCH, Weinheim, 2007.
[21] R.F.W. Bader, H. Essen, The characterization of atomic interactions, J. Chem. Phys. 80 (1984) 1943–1960.
[22] Y.A. Abramov, On the possibility of kinetic energy density evaluation from the experimental electron density distribution, Acta Cryst. A53 (1997) 264–272.
[23] O. Gálvez, P.C. Gómez, L.F. Pacios, Approximate kinetic energy density for intermolecular regions in hydrogen bond dimers, Chem. Phys. Lett. 337 (2001) 263–268.
[24] C. Gatti, Chemical bonding in crystals: new directions, Z. Kristall. 220 (2005) 399–457.
[25] E. Espinosa, E. Molins, Retrieving interaction potentials from the topology of the electron density distribution: the case of hydrogen bonds, J. Chem. Phys. 113 (2000) 5686–5694.
[26] E. Espinosa, I. Alkorta, I. Rozas, J. Elguero, E. Molins, About the evaluation of the local kinetic, potential and total energy densities in closed-shell interactions, Chem. Phys. Lett. 336 (2001) 457–461.
[27] G.V. Gibbs, D. Jayatilaka, M.A. Spackman, D.F. Cox, K.M. Rosso, Si–O bonded interactions in silicate crystals and molecules: a comparison, J. Am. Chem. Soc. 110 (2006) 12678–12683.
[28] A.D. Becke, K.E. Edgecombe, A simple measure of electron localization in atomic and molecular systems, J. Chem. Phys. 92 (1990) 5397–5403.
[29] A. Savin, A.D. Becke, J. Flad, R. Nesper, H. Preuss, H.G. von Schnering, A new look at electron localization, Angew. Chem. Int. Ed. 30 (1991) 409–412.
[30] B. Silvi, A. Savin, Classification of chemical bonds based on topological analysis of electron localization functions, Nature 371 (1994) 683–686.
[31] B. Silvi, How topological partitions of the electron distributions reveal delocalization, Phys. Chem. Chem. Phys. 6 (2004) 256–260.
[32] L.F. Pacios, A theoretical study of the intramolecular interaction between proximal atoms in planar conformations of biphenyl and related systems, Struct. Chem. 18 (2007) 785–795.
[33] A. Martín Pendás, E. Francisco, M.A. Blanco, Electron–electron interactions between ELF basins, Chem. Phys. Lett. 454 (2008) 396–403.
[34] R.D. Levine, in: R.D. Levine, M. Tribus (Eds.), The Maximum Entropy Formalism, MIT Press, Cambridge (MA), 1979.
[35] M. Hô, R.P. Sagar, J.M. Pérez-Jordá, V.H. Smith, R.O. Esquivel, A numerical study of molecular information entropies, Chem. Phys. Lett. 219 (1994) 15–20.
[36] M. Hô, D.F. Weaver, V.H. Smith, R.P. Sagar, R.O. Esquivel, Calculating the logarithmic mean excitation energy from the Shannon information entropy of the electronic charge density, Phys. Rev. A 57 (1998) 4512–4517.
[37] J.C. Ramírez, J.M. Hernández-Pérez, R.P. Sagar, R.O. Esquivel, M. Hô, V.H. Smith, Amount of information present in the one-particle density matrix and the charge density, Phys. Rev. A 58 (1998) 3507–3515.
[38] M. Hô, V.H. Smith, D.F. Weaver, C. Gatti, R.P. Sagar, R.O. Esquivel, Molecular similarity based on information entropies and distances, J. Chem. Phys. 108 (1998) 5469–5475.
[39] R.F. Nalewajski, R.G. Parr, Information theory, atoms in molecules, and molecular similarity, Proc. Natl. Acad. Sci. U.S.A. 97 (2000) 8879–8882.
[40] R.F. Nalewajski, Entropic measures of bond multiplicity from the information theory, J. Phys. Chem. A 104 (2000) 11940–11951.
[41] S. Liu, On the relationship between densities of Shannon entropy and Fisher information for atoms and molecules, J. Chem. Phys. 126 (2007), 191107/1-3.
[42] P. Politzer, D.G. Truhlar (Eds.), Chemical Applications of Atomic and Molecular Electrostatic Potentials, Plenum, New York, 1984.
[43] J.S. Murray, P. Politzer, in: P.v.R. Schleyer (Ed.), Encyclopedia of Computational Chemistry, vol. 2, Wiley, New York, 1998.
[44] P. Politzer, J.S. Murray, The fundamental nature and role of the electrostatic potential in atoms and molecules, Theor. Chem. Acc. 108 (2002) 134–142.
[45] Y.G. Ma, P. Politzer, Calculation of electrostatic and polarization energies from electron densities, J. Chem. Phys. 120 (2004) 3152–3157.
[46] L.F. Pacios, Changes of electron properties in the formation of hydrogen bonds, in: S.J. Grabowski, J. Leszczynski (Eds.), Hydrogen Bonding—New Insights, Springer, Dordrecht, 2006, pp. 109–148.
[47] H.L. Schmider, A.D. Becke, Chemical content of the kinetic energy density, J. Mol. Struct. (Theochem.) 527 (2000) 51–61.
[48] H.L. Schmider, A.D. Becke, Two functions of the density matrix and their relation to the chemical bond, J. Chem. Phys. 116 (2002) 3184–3193.
[49] V. Tsirelson, A. Stash, Analyzing experimental electron density with the localized-orbital locator, Acta Cryst. B58 (2002) 780–785.
[50] H. Jacobsen, Localized-orbital locator (LOL) profiles of chemical bonding, Can. J. Chem. 86 (2008) 695–702.
[51] E.F. Pettersen, T.D. Goddard, C.C. Huang, G.S. Couch, D.M. Greenblatt, E.C. Meng, T.E. Ferrin, UCSF Chimera—a visualization system for exploratory research and analysis, J. Comput. Chem. 25 (2004) 1605–1612 (www.cgl.ucsf.edu/chimera).
[52] Jmol: an open-source Java viewer for chemical structures in 3D (www.jmol.org).
[53] W.L. DeLano, The PyMOL Molecular Graphic System (2002) (www.pymol.org). Starting version 1.0, PyMOL was no longer free. However, as the author announces in the web site, older builds (pre-1.0) are still freely accessible.
[54] W. Humphrey, A. Dalke, K. Schulten, VMD—visual molecular dynamics, J. Mol. Graphics 14 (1996) 33–38 (www.ks.uiuc.edu/Research/vmd).
[55] T. Williams, C. Kelley, Gnuplot, an interactive plotting program. Version 4.2 (sourceforge.net/projects/gnuplot).
[56] G.A. Jeffrey, An Introduction to Hydrogen Bonding, Oxford University Press, New York, 1997.
[57] L.F. Pacios, L. Gómez, Conformational changes of the electrostatic potential of biphenyl: a theoretical study, Chem. Phys. Lett. 432 (2006) 414–420.